Single-mode nonlinear Langevin emulation of magnetohydrodynamic turbulence

Riddhi Bandyopadhyay,* William H. Matthaeus,† and Tulasi N. Parashar
Department of Physics and Astronomy and Bartol Research Institute, University of Delaware, Newark, Delaware 19716, USA

(Received 15 February 2018; published 30 May 2018)

Based on the Langevin equation of Brownian motion, we present a simple model that emulates a typical mode in incompressible magnetohydrodynamic turbulence, providing a demonstration of several key properties. The model equation is consistent with von Kármán decay law and Kolmogorov's symmetries. We primarily focus on the behavior of inertial range modes, although we also attempt to include some properties of the large-scale modes. Dissipation scales are not considered. Results from the model are compared with results from published direct numerical simulations.

DOI: 10.1103/PhysRevE.97.053211

I. INTRODUCTION

Turbulence, whether in a hydrodynamic, magnetohydrodynamic (MHD), or weakly collisional plasma, is characterized by nonlinear effects that produce complex observable signatures. In strong turbulence the dynamics recorded in individual measurements become sufficiently complex that the underlying degrees of freedom are often treated as random variables. This type of behavior would be expected, for example, in pointwise measurements of velocity, in strong turbulence, and increasingly so at large mechanical or magnetic Reynolds numbers. Much of turbulence theory proceeds through a *statistical* characterization of this behavior. Dissipation and linear effects such as waves may act to attenuate, organize, and modify the intensity of the nonlinear effects, thus modifying the statistical characterization. Here we are concerned with the particular problem of modeling statistics of magnetoydrodynamic turbulence in the presence of an externally supported mean magnetic field. We employ a simple model to demonstrate stochastic behavior of an inertial range Fourier mode, while it also engages in wavelike couplings associated with the mean magnetic field. Rather than attempting a formal analysis, we develop a model starting with a simple stochastic differential equation, the Langevin equation. After suitable modifications, we arrive at a model with two real degrees of freedom and a nonlinear damping force. The results validate the model design and reproduce several basic features of the MHD turbulence cascade. We view the purpose of a simple model such as the present one as demonstrating salient statistical properties of MHD turbulence rather than either predicting or explaining physical effects. In this way the purpose parallels that of the Langevin formalism, which is well known to demonstrate properties of Brownian motion.

II. BACKGROUND

The Langevin equation provides a reasonable starting point to represent certain stochastic properties of turbulence and turbulent transport. A classical result [1] is that the Langevin equation demonstrates the relaxation of a particle with an initial peculiar velocity to a state consistent with thermal equilibrium, and a Maxwellian (Gaussian) distribution. It follows that the displacements represent an instance of Brownian motion. The statistics of solutions to the Langevin equation formally obey a Fokker -Planck equation [1], which links this approach to many possible applications in diffusion and turbulence theory. It has been shown that even the linear damping Langevin formulation can form the basis for representation of the more complex physics occurring in turbulence. For example, Beck [2] showed that a linear Langevin formulation with chaotic forcing can describe the turbulence statistics of inertial range velocity increments. Analysis of a linear Langevin model incorporating oscillations associated with an applied magnetic field was carried out by Balescu *et al.* [3] for application to charged particle diffusion. TenBarge *et al.* [4] employed such a damped, driven linear oscillator as a method for driving plasma simulation. These studies represent antecedents to the approach and goals of the present work.

The random behavior of turbulent fields in real space is mirrored by the random behavior of its Fourier modes. This relationship becomes direct in a simple spatially periodic model representation of homogeneous turbulence. Relying in each case on an assumption of ergodicity, Gibbsian statistical mechanics [5] has been fruitfully applied to the ideal, finite-dimensional (truncated) Galerkin model of both hydrodynamic and MHD turbulence [6–8]. The impressive accuracy of the Gibbsian predictions for various wave-number spectra in these models provides affirmative support to the assumption of ergodicity of the real and imaginary parts of the Fourier amplitudes of velocity and, where applicable, magnetic fields.[1]

The stochastic behavior of individual Fourier degrees of freedom survives into the regime of driven, dissipative high Reynolds number MHD turbulence (e.g., [12]). However, when

*riddhib@udel.edu
†whm@udel.edu

[1]Long-wavelength modes sometimes exhibit *broken ergodicity* [9,10] associated with degeneracy of very large-scale degrees of freedom. Analysis of longer simulations has led to the suggestion that over very long timescales, ergodicity is restored [11].

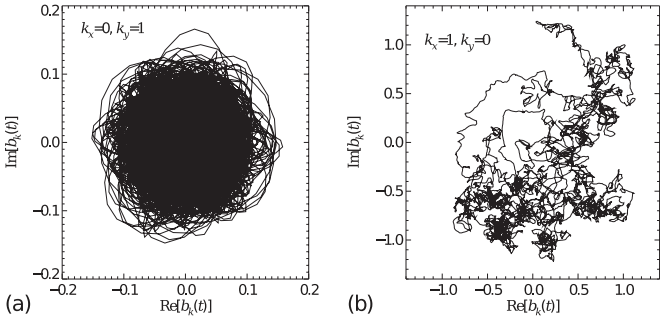

FIG. 1. Phase plane trajectories over time of two Fourier modes. Left: Mode with a high degree of wavelike behavior; right: mode exhibiting very stochastic behavior and no indication of wavelike behavior. (Adapted from Dmitruk *et al.*, 2009 [12].)

MHD turbulence evolves in the presence of an externally supported dc magnetic field, wave motions are induced, including the Alfvén wave, which survives to the incompressible limit. Wave propagation itself does not cause stochastic behavior, but rather induces an orderly rotation in the complex (Re,Im) phase plane. This contrast in behavior is illustrated in Fig. 1, which shows the time history- of the real and imaginary parts of the Fourier amplitude of a single Cartesian magnetic-field component, in a driven, dissipative MHD simulation [12]. It is apparent that one of these trajectories acts more like a constrained random walk, while the other admits a stronger sense of rotation as it is more dominantly influenced by the dc magnetic field. Demonstrating the balance and transition between these two types of behavior by varying control parameters for inertial range modes is a major goal in the present paper.

Stochastic behavior of a dynamical system motivates the development of statistical theories that invoke ergodicity, e.g., the property that permits replacement of ensemble averages by time averages. The stochastic aspects of MHD or plasma dynamics might become less prominent for certain modes when an applied magnetic field of sufficient strength is present. In applications that invoke "critical balance," wave and nonlinear timescales are often set equal to one another, as a reflection of this balance. In some related approaches, wave activity is presumed to be the dominant feature, and nonlinear effects are computed using perturbation theory. In formal weak turbulence theory, the leading order behavior is that of a wave, and nonlinearities that give rise to turbulence occur as next order corrections. Variations of this idea, often less formally implemented, include the "wave turbulence" approach [13–17] that models finite amplitude plasma turbulence by approximating turbulent fluctuations as superposition of randomly-phased linear wave modes. This "quasilinear premise" performs well in the case of weak turbulence, and it is argued to remain somewhat valid even in strong turbulence (as in the case of *Goldreich and Sridhar*'s critical balance theory).

For linear waves, the dynamics of a specified Fourier mode is expected to be that of a stochastic oscillator rather than of a simple harmonic oscillator with a characteristic frequency, e.g., as pointed out by Matthaeus *et al.* [18]. For Alfvénic turbulence, TenBarge *et al.* [4] attempted to model the effect of large-scale modes, greater than the simulation system size, by coupling individual Fourier modes $\mathbf{z}^{\pm}(\mathbf{k})$ to an oscillating Langevin antenna. Dmitruk *et al.* [19] constructed a phenomenological model based on reduced MHD to describe the driving of turbulence in the open line regions of the corona, incorporating both wave propagation effects, and models for strong nonlinearity. More complex turbulence models such as these may clearly benefit from improved simple schemes to drive them at large scales or even in the inertial range. This provides a practical motivation for development in the present paper of an elementary model designed to emulate the statistics of MHD turbulence. Clearly there are a wide range of models and applications in which the relative balance between wave activity and stochastic behavior become very important. Besides these two disparate qualitative behaviors, one might expect the relative influence of driving and dissipation to enter as well. Our motivation in developing the present model is to provide a tractable simple dynamical model that demonstrates these effects quantitatively with some level of consistency with turbulence solutions obtained by much more demanding direct numerical simulation (DNS) approaches.

The outline of the paper is as follows: in Sec. III, we build up the basic equations. In Sec. IV A, we model the nonlinear dissipation and Alfvénic wave term. In Sec. IV B, we normalize the equations. In Sec. IV C, we enforce Kolmogorov's symmetries for inertial scale modes. In Sec. IV D, we build in some scaling rules for the large-scale modes. In Sec. V, we discuss the numerical details. Section VI contains our results. We discuss some of the previous similar schemes and conclude in Sec. VII.

III. LANGEVIN AND SINGLE-MODE MODELS

The one-dimensional Langevin equation describing the Brownian motion of a particle is given by

$$\frac{du}{dt} = -\alpha u + g(t), \tag{1}$$

where u is the velocity of the particle. A systematic linear drag term $-\alpha u$ represents the friction and a fluctuating part $g(t)$ models the random kicks experienced by the particle from the surrounding medium. A Gaussian white noise is usually used for $g(t)$ [1,20].

The Langevin equation and its solutions have many interesting properties and applications. Of historical importance is that its solutions provide a useful description of Browninan motion [1,21,22]. One may also readily show that its solutions are equivalent to solutions of a Fokker-Planck equation [20], and as such it can be related to various problems in diffusion theory and in approaches to equilibrium distributions. The addition of an oscillatory degree of freedom is quite relevant to the present model, and was introduced [3] to describe charge particle collisional diffusion including gyration in a uniform large-scale magnetic field.

Our specific goal is to model the dynamical behavior of a single Fourier mode in the inertial range of MHD turbulence. As such, the physical structure and appropriate normalization of the basic incompressible model will be relevant. The equations of incompressible MHD can be expressed in terms

of the Elsässer variables, $\mathbf{z}^{\pm} = \mathbf{u} \pm \mathbf{b}/\sqrt{4\pi\rho}$, as

$$\frac{\partial \mathbf{z}^{\pm}}{\partial t} = \pm \mathbf{v_A} \cdot \nabla \mathbf{z}^{\pm} - \mathbf{z}^{\mp} \cdot \nabla \mathbf{z}^{\pm} - \frac{\nabla P}{\rho_0} - \mu \nabla^2 \mathbf{z}^{\pm}, \quad (2)$$

where $\mathbf{u}$ and $\mathbf{b}$ are velocity and magnetic-field fluctuations, respectively. $\mathbf{v_A}$ is the Alvén velocity defined as $\mathbf{v_A} = \mathbf{B_0}/\sqrt{4\pi\rho_0}$, where $\mathbf{B_0}$ is the mean magnetic field. P is the total pressure (thermal+magnetic), ρ_0 is the constant density, and μ is the viscosity, assumed to be equal to the resistivity. The quadratic nonlinear term, $\mathbf{z}^{\mp} \cdot \nabla \mathbf{z}^{\pm}$ and pressure term, $\nabla P/\rho_0$ are responsible for transferring energy from large scales, into and through the inertial range. The plasma also responds to the linear term, $\mathbf{v_A} \cdot \nabla \mathbf{z}^{\pm}$, which induces wavelike dynamics. The last term, $\mu \nabla^2 \mathbf{z}^{\pm}$, is responsible for dissipation, and for large Reynolds numbers, this term is negligible except at very small scales. For description of inertial range scales ($\gg$ dissipation range scales), the explicit dissipation makes no contribution; its influence is manifested in the continual transfer of energy toward the smaller scales. In quasisteady conditions the transfer due to eddy motions will balance the viscous effects at the dissipation scales, and therefore it is natural to suppose that inertial range eddies provide a kind of effective dissipation, or eddy viscosity.

A simple model was introduced by Dmitruk *et al.* [23] to approximate the average damping experienced by a typical mode in the inertial range, due to the net effect of all smaller scale modes. Writing the MHD equations for a typical or representative mode at a selected scale ℓ, the model proceeds to account for nonlinear effects in a way that involves only the amplitude at scale ℓ in accord with Kolmogorov's scale locality hypothesis. The nonlinearity takes the form of a quadratic drag force that is consistent with a Taylor–von Kármán decay law for MHD [24], and is a close relative of an eddy viscosity. This approach will be incorporated below.

IV. DEVELOPMENT OF THE MODEL

We begin with the assumption that the effects of nonlinearity are principally *local in scale*. Then a single Fourier mode (velocity or magnetic) residing in the inertial range, experiences a random net input of energy from the larger scales, while it dissipates by transferring energy to smaller scales. On average, the input and dissipation balance, so that there is no secular pileup of energy at any scale (no buildup of spectral amplitude at any wave number). Therefore, in analogy with the Langevin equation, Eq. (1), we write a model equation for the velocity (and magnetic) fluctuation at length scale l,

$$\frac{\partial u_l}{\partial t} = -\alpha u_l + g_l(t). \quad (3)$$

Here, we represent both velocity and magnetic fluctuation at length scale l by u_l for convenience. Note that unlike Eq. (1), the fluctuating part $g_l(t)$ in Eq. (3) is not Gaussian white noise, but a chaotic force changing on a typical timescale t_c (see Sec. V for more discussion). The amplitude of $g_l(t)$ as well as the timescale t_c are expected to change with length scale l. In steady-state MHD turbulence, usually a forcing function acts at some large-scale L which excites the nearby modes. A mode deep in the inertial range does not feel the same driving force. Rather, the influence of the force is cascaded by the larger scale couplings, through many intermediate modes, down to the scale of interest l. Here, we represent the driving felt at length scale l by the term $g_l(t)$.

We remark that Eq. (3), which remains formally a Langevin equation, was also adopted by Beck [2] for describing (or, as here, emulating) properties of turbulence. In contrast to the present case, Beck's Langevin model [Eq. (3)] is written for the evolution of an inertial range velocity *increment*, and the focus is on constructing a model that can reproduce scaling of higher-order structure functions in the inertial range. Scaling (i.e., intermittency) is introduced in the model through use of a forcing function based on a logistic map scheme. As shown presently, our approach is quite different.

A. Modeling of nonlinearity and Alfvén waves

To modify the classical Langevin equation, Eq. (1), we start with the dissipative term $-\alpha u_l$. From the von Kármán similarity hypothesis, extended to MHD, we expect that [24,25]

$$\frac{du_l^2}{dt} \propto \frac{u_l^3}{l}. \quad (4)$$

Accordingly, we modify the linear drag term in Eq. (3) so that it becomes nonlinear, as

$$\alpha u_l \to \frac{C}{l}|u_l|u_l, \quad (5)$$

and the model equation, Eq. (1), becomes

$$\frac{\partial u_l}{\partial t} = -\frac{C}{l}|u_l|u_l + g_l(t). \quad (6)$$

In this equation, if we set the forcing term to zero, the energy goes as

$$\frac{\partial |u_l|^2}{\partial t} \sim -\frac{C}{l}|u_l|^3. \quad (7)$$

The constant C appearing in Eqs. (19) and (27), is expected to be close to the Taylor–von Kármán decay constant, extended to MHD [24,26]. The value of C has been measured to be around 0.5 for hydrodynamic turbulence [27]. In MHD and kinetic plasmas, recent studies show hints of a universal decay rate at large Reynolds number, with a decay constant close to unity [28,29]. We use a value of $C = 0.5$ in this study.

MHD turbulence also supports Alfvén waves, most easily described by introducing a uniform mean magnetic field $\mathbf{B_0}$. When present, the Alfvén wave frequencies are $\omega \sim \mathbf{k} \cdot \mathbf{V_A} \sim k B_0 \cos\theta$. To accommodate the physics of these incompressible MHD waves in the present model, we introduce a new term to the model equation, Eq. (6), which becomes

$$\frac{\partial u_l}{\partial t} = i\omega u_l - \frac{C}{l}|u_l|u_l + g_l(t). \quad (8)$$

Here $i = \sqrt{-1}$, and since $l \sim 1/k$, we have $\omega \sim B_0 \cos\theta/l$. Here B_0 is the characteristic magnetic-field strength in Alfvén speed units. Note that the dependent variable u_l in Eq. (6) has become complex, and represents a typical Fourier amplitude, and not simply a typical speed at scale ℓ. This is commensurate with the interpretation of a typical Fourier mode in Dmitruk *et al.* [19].

Using this interpretation and our notation, $|u_l|^2$ can be equated to (twice) the energy per unit mass in fluctuations at a

scale l in turbulence. To make this correspondence we view $|u_l|$ as a contribution to a full (omnidirectional) spectrum $E(k)$ that varies over wave number k. By construction, with $k \to 1/l$,

$$|u_l|^2 = kE(k), \quad \text{or} \quad E(k) = l|u_l|^2 \tag{9}$$

and therefore we can directly obtain a spectrum from u_l by varying l.

B. Normalization

In order to compare the results from our model equation with other systems like DNS, we normalize our equations in a physically revealing way. In the process, we shall also specify the characteristic timescale (correlation timescale) that associated with $g_l(t)$. The following treatment will also enable us to specify an appropriate scale dependence of g_l, i.e., $g_l(t) = g(l,t)$.

To normalize Eq. (8), we select a large-scale length λ, associated with which, we have a typical velocity (or magnetic) fluctuation $u_{0\lambda}$. This establishes the characteristic timescale $\tau_{0\lambda}$ through

$$\tau_{0\lambda} = \frac{\lambda}{u_{0\lambda}}. \tag{10}$$

The scale λ will represent the energy containing scale, and so $\tau_{0\lambda}$ is the system eddy turnover time. Similarly, at another length scale of interest l, where for the inertial range, $l < \lambda$, there is typical velocity u_{0l} and an implied timescale τ_{0l} such that

$$u_{0l} = \frac{l}{\tau_{0l}}. \tag{11}$$

We would like to emphasize the difference between u_l and u_{0l} or τ_l and τ_{0l}. u_l and τ_l are the instantaneous velocity fluctuation and timescale at length scale l, while u_{0l} and τ_{0l} are the *typical* velocity and timescale at same length scale l. With this, we normalize different quantities as follows:

$$u_l = u_{0\lambda}\widetilde{u}_l, \quad t = \tau_{0\lambda}\widetilde{t}, \quad l = \lambda\widetilde{l}. \tag{12}$$

Further, we write g_l as

$$g_l = \left(\frac{u_{0l}}{\tau_{0l}}\right)\widetilde{g}, \tag{13}$$

where $\widetilde{g}$ is a dimensionless order-one random function of time. The quantities with $\widetilde{\ }$ in the overhead are all dimensionless, with $\widetilde{u}_l$ the dependent variable, $\widetilde{t}$ the independent variable, and $\widetilde{l}$ a fixed constant during time integration.

Plugging Eqs. (12) and (13) into Eq. (8),

$$\frac{u_{0\lambda}}{\tau_{0\lambda}}\frac{\partial\widetilde{u}_l}{\partial\widetilde{t}} = i\omega u_{0\lambda}\widetilde{u}_l - \frac{C}{\widetilde{l}\lambda}u_{0\lambda}^2|\widetilde{u}_l|\widetilde{u}_l + \frac{u_{0l}}{\tau_{0l}}\widetilde{g}, \tag{14}$$

$$\frac{\partial\widetilde{u}_l}{\partial\widetilde{t}} = i(\omega\tau_{0\lambda})\widetilde{u}_l - \frac{C}{\widetilde{l}}|\widetilde{u}_l|\widetilde{u}_l + \left(\frac{u_{0l}\tau_{0\lambda}}{\tau_{0l}u_{0\lambda}}\right)\widetilde{g}. \tag{15}$$

Now, we note that the wave timescale can also be written in eddy turnover time units as

$$\omega\tau_{0\lambda} = k_\parallel B_0\tau_{0\lambda} = (k_\parallel\lambda)\left(\frac{B_0}{u_{0\lambda}}\right) = \widetilde{k}_\parallel\widetilde{B}_0 = \widetilde{\omega}.$$

Therefore, we have

$$\frac{\partial\widetilde{u}_l}{\partial\widetilde{t}} = i\widetilde{\omega}\widetilde{u}_l - \frac{C}{\widetilde{l}}|\widetilde{u}_l|\widetilde{u}_l + \left(\frac{u_{0l}\tau_{0\lambda}}{\tau_{0l}u_{0\lambda}}\right)\widetilde{g}. \tag{16}$$

C. Inertial range modes

In this section we aim to recover the Kolmogorov scaling $E(k) \sim k^{-5/3}$ for the inertial range in a systematic way. For l in the inertial range, following Kolmogorov [30], we enforce the following symmetries in Eq. (16):

$$\left(\frac{\tau_{0l}}{\tau_{0\lambda}}\right) = \left(\frac{l}{\lambda}\right)^{2/3}, \tag{17}$$

$$\left(\frac{u_{0l}}{u_{0\lambda}}\right) = \left(\frac{l}{\lambda}\right)^{1/3}. \tag{18}$$

So, Eq. (16) becomes

$$\frac{\partial\widetilde{u}_l}{\partial\widetilde{t}} = i\widetilde{\omega}\widetilde{u}_l - \frac{C}{\widetilde{l}}|\widetilde{u}_l|\widetilde{u}_l + \widetilde{l}^{-1/3}\widetilde{g}. \tag{19}$$

This is the equation we propose for emulation of inertial range modes.

From Eq. (19) we can write

$$\frac{\partial|\widetilde{u}_l|^2}{\partial\widetilde{t}} = -2\frac{C}{\widetilde{l}}|\widetilde{u}_l|^3 + \widetilde{l}^{-1/3}(\widetilde{g}\widetilde{u}_l^* + \widetilde{g}^*\widetilde{u}_l). \tag{20}$$

In the steady state, $\frac{\partial|\widetilde{u}_l|^2}{\partial\widetilde{t}} = 0$ and $|\widetilde{g}| \sim 1$. So,

$$\frac{C}{\widetilde{l}}|\widetilde{u}_l|^3 \sim \widetilde{l}^{-1/3}|\widetilde{u}_l|, \tag{21}$$

$$|\widetilde{u}_l|^2 \sim \widetilde{l}^{2/3}, \tag{22}$$

which is consistent with Kolmogorov's theory [see Eq. (18)]

The random term $\widetilde{g}$ fluctuates randomly in time and it has a correlation time t_c associated with it. For a particular mode to be driven efficiently, one expects that the correlation time, t_c, has to be of the same order of the local turbulence timescale (τ_l) (see [4,31,32]). Therefore we equate the correlation time with the local turbulence timescale,

$$\widetilde{t}_c = \frac{\tau_{0l}}{\tau_{0\lambda}}. \tag{23}$$

D. Large-scale modes

Large-scale modes do not exhibit universal scaling in three-dimensional MHD turbulence. Still, there are some common characteristics observed in large-scale modes in MHD turbulence. One such feature is the presence of $1/f$ or "flicker noise" in the lowest wave-number mode. The presence of a low-frequency $1/f$ signal in turbulent systems was investigated in some detail by Dmitruk and Matthaeus [33], and Dmitruk *et al.* [34]. A heuristic reasoning was proposed in [33] and [34] to explain the occurrence of low-frequency $1/f$ noise in the lowest wave-number mode. The lowest wave-number mode, say $k = 1$, interacts with other modes via triadic interaction of the (schematic) form

$$\frac{\partial b(k=1)}{\partial t} \sim i\sum_{p+q=1} u(q)b(p), \tag{24}$$

where $b(k=1)$ represents the first mode, and $u(p)$,$u(q)$ are generic Fourier mode amplitudes. If the interaction is nonlocal, $p,q \gg k=1$, $p \sim q$, the timescale from the right-hand side of Eq. (24) is $[u(q)b(q)/b(k=1)]^{-1}$, which is much longer than the local eddy turnover timescale since $u(q),b(q) \ll u(k=1)$, $b(k=1)$. It is worth mentioning here that a $1/f$ signal has also been observed in other turbulent plasma systems such as interplanetary magnetic field [35], solar corona [36], and photosphere [37], although the source of the $1/f$ signal in these systems may be (at least partially) different from the above heuristic reasoning.

One might anticipate the emergence of low-frequency $1/f$ noise in a Langevin model such as Eq. (19), if, for the case in question, one imposes a timescale (t_c) of the stochastic forcing $\widetilde{g}$, that is much greater than the local eddy turn over time ($l/|u_l|$). We demonstrate this in the following way. We postulate (in an *ad hoc* fashion) that for the large-scale modes with $l > \lambda$, the timescale goes as the square of length scale. So, we have

$$\left(\frac{\tau_{0l}}{\tau_{0\lambda}}\right) = \left(\frac{l}{\lambda}\right)^2. \tag{25}$$

We further assume that in this range of scales, the characteristic speeds are simply proportional to the respective characteristic lengths, i.e.,

$$\left(\frac{u_{0l}}{u_{0\lambda}}\right) = \left(\frac{l}{\lambda}\right). \tag{26}$$

So, for large-scale modes, Eq. (16) becomes

$$\frac{\partial \widetilde{u}_l}{\partial \widetilde{t}} = i\widetilde{\omega}\widetilde{u}_l - \frac{C}{\widetilde{l}}|\widetilde{u}_l|\widetilde{u}_l + \widetilde{l}^{-1}\widetilde{g}. \tag{27}$$

Also, we equate the correlation time of the forcing, t_c, with the timescale in Eq. (25),

$$\widetilde{t}_c = \frac{\tau_{0l}}{\tau_{0\lambda}} = \left(\frac{l}{\lambda}\right)^2. \tag{28}$$

We choose λ = the length scale which separates the large-scale modes from the inertial modes. So, for $l < \lambda$, we use Eq. (19) and for $l > \lambda$, we use Eq. (27). Note that in this notation, the nondimensional wave number $\widetilde{k} = 1/\widetilde{l} = \lambda/l$ can be greater (inertial scales), equal, or less (large scales) than 1. From now on, for convenience, we will use the variables without the $\widetilde{\ }$ in the overhead.

V. NUMERICAL DETAILS

For numerical implementation, Eqs. (19) and (27) are advanced in time using the fourth-order Runge-Kutta (RK4) scheme. The nondimensional wave number k varies logarithmically from 0.3 to 30. The total number of points in wave-number space is 128. The variables used in Eq. (19) have a real and an imaginary component. Numerically, we determine the random forcing term g as

$$g(t) = mg(t-\Delta t) + \sqrt{(1-m^2)}r(t). \tag{29}$$

The value of g at the $(n+1)$th step, i.e., at time $t=(n+1)\Delta t$, is generated from the previous value (at the nth step) of g and a random number, r. The constant m is a memory constant that relates how the sequence "remembers" the past values. The random number r satisfies the following properties:

$$\langle r \rangle = 0, \tag{30}$$

$$\langle r(t)r(t') \rangle = \delta(t-t'). \tag{31}$$

These are satisfied by a normalized Gaussian random number generator. With these properties one can derive the correlation function for g (see [38]),

$$G_c(\tau) = \langle g(t)g(t+\tau) \rangle = e^{-\tau/t_c}, \tag{32}$$

$$\text{and} \quad t_c = \frac{\Delta t}{1-m}. \tag{33}$$

These results are valid in the appropriate limit, with, e.g., $\Delta t \to 0$, and $n \to \infty$, such that $\tau = n\Delta t$ remains constant, t similarly defined, $m \to 1$ with t_c constant, and Eqs. (30) and (31) enforced. Also note that the real and imaginary parts of the random term $\widetilde{g}$ in Eq. (19) are independent of each other. That is, at each time step the real and imaginary components are determined from Eq. (29) with same memory function m, but employing different random numbers.

We choose a time step $\Delta t = 10^{-3}$, and we run the simulation for 10^9 time steps, i.e., 10^3 units of nondimensionalized time.

For calculating frequency spectra, we use an ensemble average of ten independent time series with random initial conditions. This helps eliminate unwanted noise in the Fourier spectrum.

VI. RESULTS

A. Isotropic case

Following the numerical method described in the preceding section, we obtain solutions for varying length scale l (reciprocal of the wave number k). For the results shown, $k\lambda$ ranges from 0.3 to 30. In this section, we consider the case $\omega = 0$, which corresponds to the situation of globally isotropic MHD with no mean magnetic field, $\mathbf{B_0} = 0$.

As a first step, we examine the relationship between the imposed correlation timescale t_c of the forcing g, with the local eddy turnover time ($\tau_{\text{eddy}} \sim l/|u_l|$), since we control the former while the latter is determined from the solution. Figure 2 shows this comparison. For the τ_{eddy} calculation, we use the time-averaged value of $|u_l|$. At smaller scales associated with the inertial range, the characteristic local nonlinear time was chosen to follow a Kolmogorov scaling [Eq. (17)] and the forcing correlation time and computed eddy turnover time are found to be almost equal. However, for the long-wavelength modes with $l > \lambda$ the imposed scaling was modified [Eq. (25)] to favor longer timescales, and we find from the solutions that $t_c \gg \tau_{\text{eddy}}$ for the lowest wave number $k\lambda = 0.3$. This establishes the long-wavelength conditions that have been argued [33] to favor generation of a $1/f$ signal in the *frequency* spectra, an issue we address below.

The distribution of energy over wave number (inverse length scale) is a central issue in turbulence, and our simple model is designed to reproduce this basic result. In contrast to hydrodynamics, the energy spectra in MHD is perennially debated and there have been a number of proposed phenomeno-

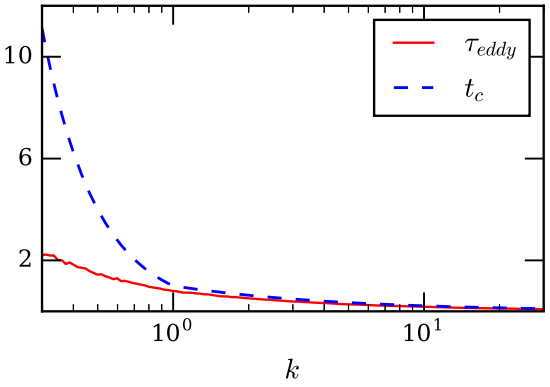

FIG. 2. Plot of correlation timescale of the stochastic forcing, t_c, along with the calculated eddy turnover time $\tau_{\text{eddy}} \sim l/|u_l|$, obtained from the model. For the τ_{eddy} calculation, we use the time-averaged value of $|u_l|$. All the variables are dimensionless as discussed in the text.

logical models (see [39] for a review). As an example, using a renormalization-group technique, Verma [40] showed that isotropic MHD should follow a $-5/3$ energy spectrum in the inertial range. Solar wind observation and DNS results also favor Kolmogorov-like spectra. In the present model, wave number k and length scale l are related simply by $k \sim 1/l$ and the energy spectrum corresponds to $E(k) \to l\langle {u_l}^2 \rangle$.

Figure 3 shows the spectrum $E(k)$ as function of wave number k using our model. Kolmogorov $k^{-5/3}$ scaling is evident at large k. At small wave numbers, $k < 1$, the spectrum scales approximately as k^{-1}; this is a consequence of the particular choice of long-wavelength timescales Eq. (25) and should not be viewed as of essential import. For each k, we have time-averaged $|u_l|^2$ to obtain $E(k)$.

The scale-dependent two-time correlation function for a full Fourier representation of the Elasässer variables is defined as

$$R(\mathbf{k},\tau) = \frac{\langle \mathbf{z}^{\pm}(\mathbf{k},t) \cdot \mathbf{z}^{\pm *}(\mathbf{k},t+\tau) + \text{c.c.} \rangle}{\langle |\mathbf{z}^{\pm}(\mathbf{k})|^2 \rangle}, \tag{34}$$

where $\langle \cdots \rangle$ represents the average over all time t, c.c. stands for complex conjugate, $\mathbf{k}$ is a specified wave vector, τ is the time lag, and $\mathbf{z}^{\pm}(\mathbf{k},t)$ is the Fourier amplitude of $\mathbf{z}^{\pm}$ at wave vector $\mathbf{k}$ at time t. Scale-dependent time correlations are well

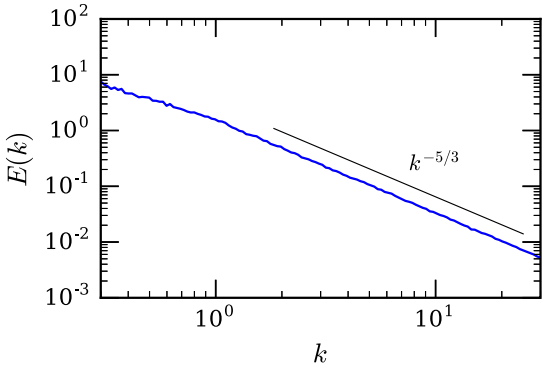

FIG. 3. Energy spectra $E(k)$ obtained from the model with $\omega = 0$. Kolmogorov scaling, $\sim k^{-5/3}$ scaling, is shown as reference.

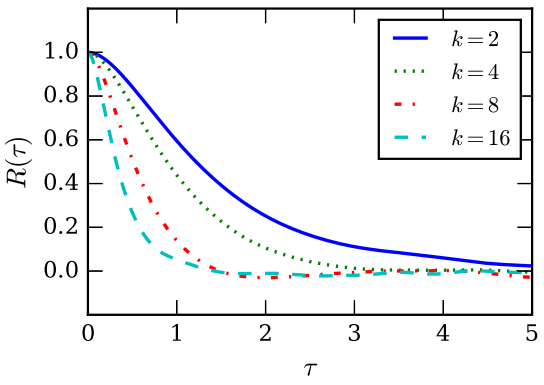

FIG. 4. Correlation function $R(\tau)$ as a function of the time lag τ for different wave numbers k.

recognized as essential elements of turbulence theory [41] including closures [42].

For our model equation, we calculate the two-time autocorrelation function as

$$R(k,\tau) = \frac{\langle u_k(t) u_k^*(t+\tau) + \text{c.c.} \rangle}{\langle |u_k|^2 \rangle}, \tag{35}$$

where it is understood that $k = 1/l$ and $u_k = u_l$. Numerically, for computing the autocorrelation function, we use the Blackman-Tukey technique [43], which gives a consistent approximation based on the formula

$$\langle |u_k|^2 \rangle R(n) = \frac{1}{M-n} \sum_{P=1}^{M-n} [u_k(P) u_k^*(P+n) + \text{c.c.}]$$
$$n = 0,1,2,\ldots,N. \tag{36}$$

Here, N is the maximum lag for which R is calculated and M is the total number of data points. Data points are separated by time step Δt. We computed the two-time correlation function obtained from solutions of the model equation for varying scale size l. The results are shown in Fig. 4. Previously, Servidio *et al.* [44] and Lugones *et al.* [45] calculated the two-point (scale-dependent) temporal autocorrelation functions for isotropic MHD turbulence. These studies found that the correlation function $R(k,\tau)$ approaches zero with different rates for different wave vector k. The higher k's decay at a faster rate compared to lower k's. Similar behavior can be seen from plots in Fig. 4. Once the calculation of $R(\tau)$ is done, we can also calculate the correlation time $\tau(k)$ as a function of effective wave number $k = 1/l$,

$$\tau(k) = \int_0^{\infty} R(\tau) d\tau. \tag{37}$$

In practice, the upper limit of the integral extends to the final time in the data record. The plots of correlation time as a function of k is shown in Fig. 5. Servidio *et al.* [44] used a best fit of six data points and found that the scaling of $\tau(k)$ with k is closer to the sweeping time τ_{sw}, which goes as k^{-1}, than the local nonlinear time τ_{nl}, which scales like $k^{-2/3}$. Lugones *et al.* [45] used more dense data points in k space and showed that, for the isotropic case, the correlation time $\tau(k)$ is close to the sweeping time $\tau_{\text{sw}} \sim k^{-1}$ for small k and it is close to the nonlinear time $\tau_{\text{nl}} \sim k^{-2/3}$ at large k values.

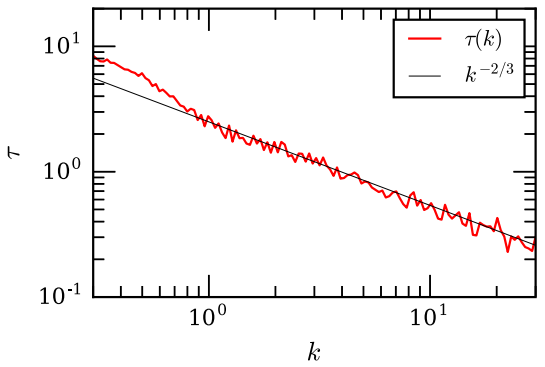

FIG. 5. Correlation time τ as a function of wave number k from the model equation. For comparison, nonlinear time, $\sim k^{-2/3}$ is shown.

In Fig. 5, we see that in the inertial range, the correlation time $\tau(k)$ scales like $k^{-2/3}$, rather than k^{-1}, as observed in isotropic MHD simulations [45]. This indicates that our model does not capture the sweeping effects properly. We discuss this issue more elaborately later in the paper.

Complementary views are provided by alternative analyses of the space-time correlations. For example, scale-dependent correlation functions, as in Eq. (34), or more specific to our model, Eq. (35), may also be Fourier analyzed in time. This leads to scale (or wave-vector) -dependent frequency spectra, examples of which are shown for model results in Fig. 6. In this figure, $P(f)$ is the square absolute value of the complex fast Fourier transform (FFT) of the time series $u_k(t)$,

$$\hat{u}_k(f) = \mathrm{FFT}[u_k(t)], \tag{38}$$

$$P(f) = |\hat{u}_k(f)|^2. \tag{39}$$

In three-dimensional, isotropic MHD, a $1/f$ signal is observed in the frequency spectra, in the largest mode, while in three-dimensional hydrodynamics, $1/f$ noise is absent, or at least weaker than MHD [33]. In Fig. 6 we show the ensemble-averaged compensated frequency space spectrum for $k = 0.3$, which is the largest mode in our system, and for one of the large modes, $k = 0.6$. We have plotted the product of frequency by spectral power, $fP(f)$, to facilitate identification of $1/f$ power. Both axes are in nondimensional units as discussed in Sec. IV B. For the $k = 0.3$ mode, $1/f$ noise appears to be

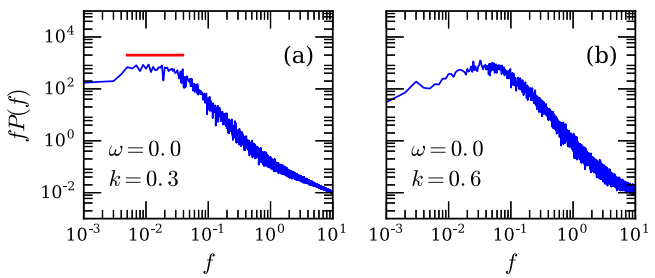

FIG. 6. Ensemble-averaged compensated frequency power spectrum. A horizontal bar in panel (a) indicates the region of approximate $1/f$ spectral behavior. No such region is prominent in panel (b).

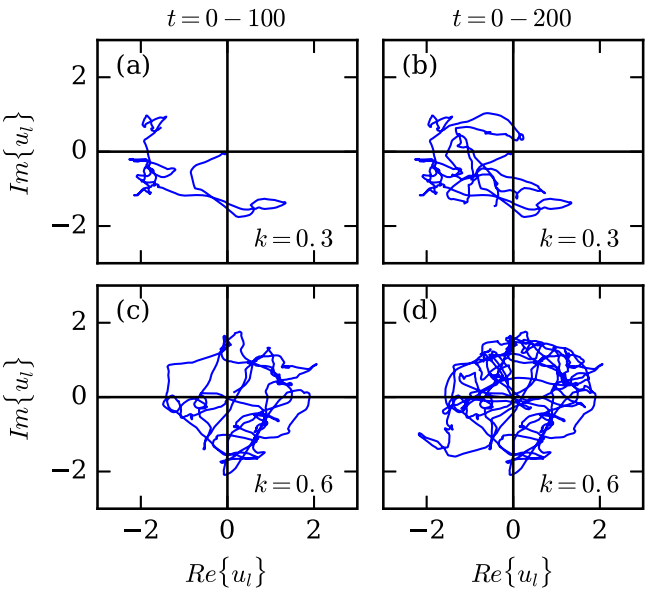

FIG. 7. Phase-space plots of $k = 0.3$ and $k = 0.6$ modes with $\omega = 0$ as obtained from the model equation. Panels (a) and (b) show the trajectory of the $k = 0.3$ mode at time $t = 0$–100 and $t = 0$–200, respectively. Panels (c) and (d) show the trajectory of the $k = 0.6$ mode at time $t = 0$–100 and $t = 0$–200, respectively.

present for more than one decade, while it is absent or at least less clear for the $k = 0.6$ mode. This is a consequence of the timescales that we imposed on the large-scale modes, given in Eq. (25). However, the result does demonstrate the plausibility of the explanation for $1/f$ noise advanced by Dmitruk *et al.* [33], as further discussed below.

Dmitruk *et al.* [34] argued that the emergence of $1/f$ fluctuations in the frequency spectra of the largest modes in MHD is related to the long-range interaction between the largest mode and the small-scale modes. The largest mode spends more time in clusters of phase space before jumping to a different region and thereby covers less area in the phase space in a given time interval, compared to the large-scale modes. This phenomenon is a manifestation of broken ergodicity [10,11] and is thought to be related to the appearance of $1/f$ noise. We analyze the phase-space diagram for the $k = 0.3$ and $k = 0.6$ modes in Fig. 7. The left and right panels in each set of figures show the evolution of the phase-space trajectory in the same intervals of time for the two modes. It is clear that in the same interval of time, the $k = 0.3$ mode covers less area of the phase space compared to the $k = 0.6$ mode. The $k = 0.6$ mode covers the phase space more uniformly compared to the $k = 0.3$ mode which mostly remains limited to the left quadrants during the time considered.

B. Anisotropic case: Effect of the imposed dc magnetic field

We perform a set of simulations of the model equation with $\omega = 0.5, 1.0, 2.0$. This may be related to MHD turbulence in the presence of a dc mean magnetic field $\mathbf{B_0}$. It is well known that turbulence in MHD with a dc field $\mathbf{B_0}$ has a strong tendency to become anisotropic, the cascade producing gradients stronger in the two directions perpendicular to $\mathbf{B_0}$, and

weaker in the parallel direction [46,47]. Physically this occurs because Alfvén wave-like couplings destructively interfere with correlations that establish nonlinear spectral transfer. This suppresses parallel spectral transfer but has no direct effect on perpendicular transfer.

The present model is in effect one-dimensional, so it is not possible to fully represent the anisotropic dynamics anticipated for a full MHD representation. However, from the developments leading to the model equation above, we can compare the frequency-dependent wave term to the nonlinear term, for example in Eq. (16). The ratio is $\frac{k_\parallel V_A}{u_l/l} = \cos\theta \frac{V_A}{u_l}$. Consequently, if we choose a scale l, a turbulence level, and a mean magnetic-field strength, then the strength of the Alfvén wave effect is controlled only by the angle θ between B_0 and $\mathbf{k}$.

While we again emphasize that a simplified one-dimensional model cannot capture the full physics of anisotropic MHD, by varying ω we can examine how changing the applied field strength (or, equivalently, the angle θ) affects the solutions.

There is another, more subtle way that wave activity may enter. Consider modes that have wave vector purely perpendicular to the direction of $\mathbf{B}_0$, so that $k_\parallel = 0$. One might naively expect that these $k_\perp$ modes (also called "2D modes") would not experience wave signatures since their intrinsic Alfvén frequency $\omega = k_\parallel B_0 = 0$. However, through nonlinear interactions, the 2D/$k_\perp$ modes are coupled to modes with nonzero $k_\parallel$ modes. Dmitruk and Matthaeus [12] studied this phenomena in some detail, finding the presence of wave activity in certain $k_\parallel = 0$ modes manifested by the appearance of Alfvén frequency peaks in the frequency spectrum of $k_\perp$ modes. Howes and Nielson [48] derived some elementary nonlinear couplings of this type by considering collision of Alvén waves in the weakly nonlinear limit. One concludes that the effective value of the Alfvén frequency ω for a mode with specified wave vector $k_\perp$ depends on which $k_\parallel$ mode interacts most dominantly. This may vary in different systems with different setups.

In principle, a Fourier mode with wave vector perpendicular to the mean magnetic-field direction can feel a frequency value anywhere in the range $0 < \omega < \infty$. However, for direct wave couplings, the increasing values of ω are qualitatively similar to the effect of increasing dc field while holding $k_\parallel$ constant or keeping the dc field constant while increasing $k_\parallel$, up to a maximum value of $k_\parallel = k = 1/l$. Indirect wave couplings may be qualitatively studied by judiciously selecting a nonzero ω for any chosen $k_\perp$ mode.

Figure 8 shows the energy spectrum plots obtained from the model for the three cases, $\omega = 0.5, 1, 2$. One may interpret this as an illustration of the anisotropic spectrum $E(k_\parallel, k_\perp)$ plotted as functions of $k_\perp$, for a series of three values of $k_\parallel$. A spectral form $E(k_\perp) \sim k_\perp^{-5/3}$ is clearly present in the inertial range.

Following the same procedure as mentioned for the $\omega = 0$ case, we calculate the two-time autocorrelation function from the model for different values of ω. Results are shown in Fig. 9. Similar to the $\omega = 0$ case, the correlation function $R(k, \tau)$ drops faster for larger k, but the disparity becomes less prominent with larger ω. This is consistent with the DNS results as found in [44,45].

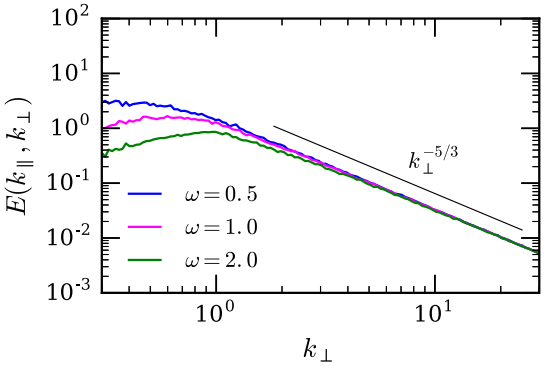

FIG. 8. Energy spectra $E(k_\parallel, k_\perp)$ vs $k_\perp$ obtained from the model with $\omega = 0.5$, 1, and 2. Kolmogorov scaling, $\sim k_\perp^{-5/3}$, is shown for reference.

An interesting observation can be made from Fig. 10. In Figs. 10(a)–10(c) we have plotted the decorrelation time τ as a function of wave number $k_\perp$, for $\omega = 0.5$, 1.0, and 2.0, respectively, as obtained from the model equation. We fit the data with nonlinear time $\tau_{\rm nl} \sim (k_\perp + k_\parallel)^{-1/3}$, for $k_\parallel$ in the ratio of 1:2:4 for the three cases $\omega = 0.5, 1.0, 2.0$. We

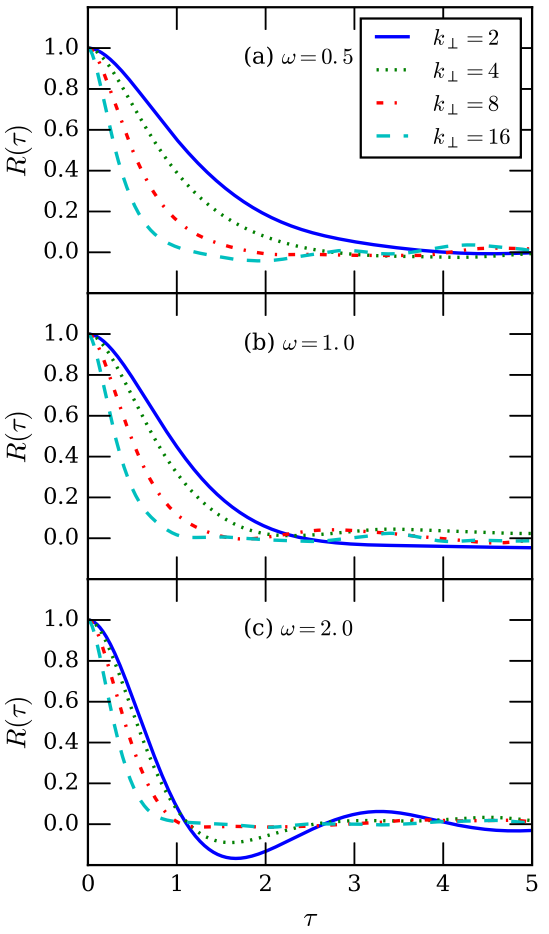

FIG. 9. Correlation function $R(\tau)$ as a function of the time lag τ for different k modes with nonzero ω. In each panel, ω is constant; (a) $\omega = 0.5$, (b) $\omega = 1$, and (c) $\omega = 2$.

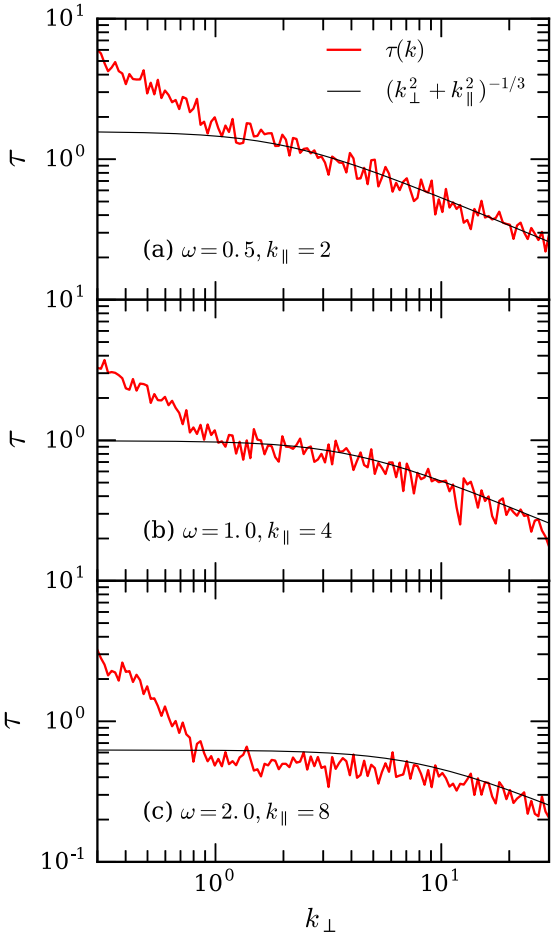

FIG. 10. Correlation time τ as a function of perpendicular wave number $k_\perp$ for different values of ω; (a) $\omega = 0.5$, (b) $\omega = 1$, (c) $\omega = 2$. The dashed curves show a fitted nonlinear time, $\sim(k_\perp^2 + k_\parallel^2)^{-1/3}$ for comparison. (a) $k_\parallel = 2.0$, (b) $k_\parallel = 4.0$, and (c) $k_\parallel = 8.0$.

found reasonably good fit for $k_\parallel = 2$, 4, and 8 for (a), (b), and (c). The fitting curves have been scaled by multiplying a constant to align with the data. Like the $\omega = 0$ case, we can compare Fig. 10 with the findings of Lugones *et al.* [45] where it was found that, for the anisotropic case, the effect of Alfvén frequency enters the decorrelation time $\tau(k)$ in a way that $\tau(k)$ follows the sweeping timescale τ_{sw} more closely than the nonlinear time τ_{nl}. As mentioned before, since we do not consider the effects of sweeping eddies in the present model, we expect the decorrelation time to scale like local nonlinear time as found in Fig. 10. We come back to the discussion on sweeping effects in Sec. VII.

Dmitruk and Matthaeus [33] showed that the $1/f$ signal appears at low frequencies in the frequency spectrum and the signal becomes stronger with increasing mean field. In Fig. 11 we show the compensated frequency spectrum obtained from the model for $\omega = 1$. Again, a clear presence of $1/f$ power can be seen in the $k = 0.3$ mode in the left panel, while the $k = 0.6$ mode shows no such scaling. Also, comparing Figs. 6(a) and 11(a), the range of $1/f$ power for the $\omega = 1.0$ case is somewhat larger than the $\omega = 0.0$ case. Therefore, it can be concluded that the $1/f$ signal becomes stronger with increasing ω, as seen in MHD simulations [33].

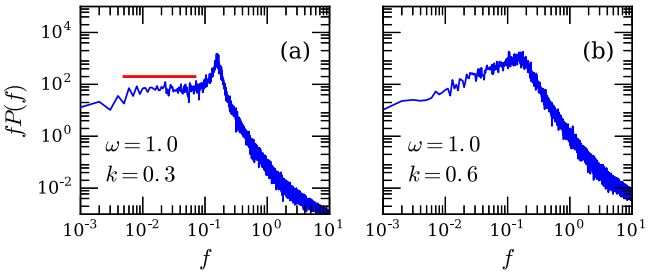

FIG. 11. Ensemble-averaged compensated frequency power spectrum. A horizontal bar in panel (a) indicates the region of approximate $1/f$ spectral behavior. No such region is prominent in panel (b).

We also show the phase-space diagram of the largest mode for the two cases $\omega = 0.5$ and $\omega = 1.0$ in Fig. 12. It is evident from the panels that the wave nature of the trajectory becomes stronger with increasing ω (compare Figs. 7 and 12). One way of quantifying the wave versus turbulent nature of a time series is through analogy to the signal-to-noise ratio (SNR) defined as [12,49]

$$\mathrm{SNR} = \log_{10}\left[\frac{P(f_0)}{P_0(f_0)}\right]. \tag{40}$$

Here f_0 is the frequency at the peak (center), corresponding to the applied frequency in the model [Eq. (16)], and $P_0(f_0)$ is a background value of the power spectrum, if the power law were continued through f_0, ignoring the peak at the wave frequency.

The meaning of this parameter is illustrated in Fig. 13.

The SNR values for the $k = 0.3$ mode for different ω, are reported in Table I. The SNR is 0 for the $\omega = 0$ case and increases monotonically for the increasing values of ω. The

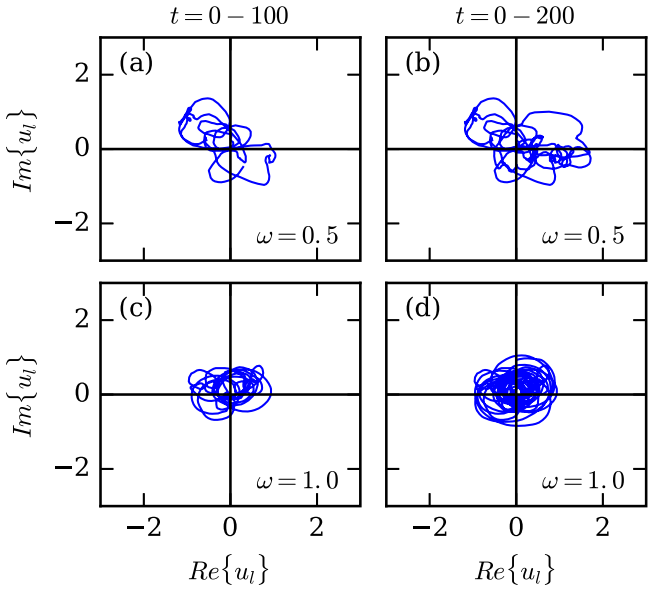

FIG. 12. Phase-space plot of the mode $k = 0.3$ for $\omega = 0.5$ and $\omega = 1$. Panels (a) and (b) show the trajectory of the $k = 0.3$ mode for $\omega = 0.5$ at time $t = 0$–100 and $t = 0$–200, respectively. Panels (c) and (d) show the trajectory of the $k = 0.3$ mode for $\omega = 1$ at time $t = 0$–100 and $t = 0$–200, respectively.

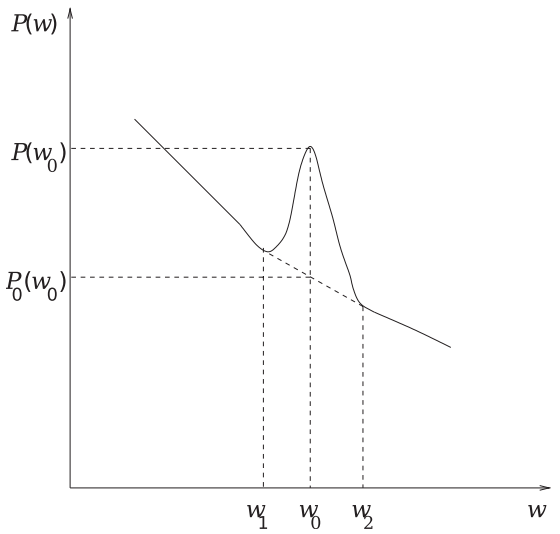

FIG. 13. Scheme for illustrating the calculation of SNR. Variable w, used in the figure, and the frequency f are related by $w = 2\pi f$. (Adapted from [12].)

fact that the phase-space trajectories become more wavelike (see Figs. 7 and 12) with noticeable peak at corresponding ω [see Fig. 11(a)] is reflected through this observation. This is again consistent with the findings based on full MHD simulations [33].

VII. DISCUSSION

In this paper, we have modified the Langevin equation of Brownian motion and the equation of Kubo-type oscillator to mimic some properties of MHD turbulence. By a systematic conglomeration of the von Karman similarity decay hypothesis, Kolmogorov symmetries, and the Langevin process of Brownian motion, the model is shown to produce some results well in agreement with DNS results. A number of similar "map" models have been proposed in the past to model hydrodynamic turbulence. Bak *et al.* [50] suggested a discrete "cellular automata" may be thought of as a "toy" turbulence model. Quantitative agreement with experimental results has been shown using Langevin-type models (see [51]). Beck proposed a series of simple cascade models based on an extension of Langevin theory to recover scaling and intermittency properties of hydrodynamic turbulence [2,52,53] (also see [54]). Similar Langevin models with complex variables with a linear term have also been used to study simple models for quantum turbulence [55,56]. However, apart from subtle differences, our model is different from the earlier models in at least two ways:

TABLE I. SNR for the $k = 0.3$ mode for different values of ω.

ω	SNR
0.0	0.0
0.5	0.44
1.0	1.64
2.0	2.30

(1) We do not introduce any cascade in our model. Different length scales evolve independently of each other, while the cascade is modeled by a correlated random forcing.

(2) For the anisotropic case, we introduce a wave term which models the Alfvén waves in MHD. This property is absent in incompressible hydrodynamic turbulence.

Due to the structure that we have imposed, the present model is able to reproduce a number of important and realistic features of MHD turbulence, at extremely low computational cost:

(i) the model obtains a Kolmogorov inertial range spectrum;

(ii) at long wavelengths, modifying a parameter to generate long correlation times, the model obtains a range of modes with $1/f$ frequency spectra; and

(iii) introduction of wave activity in the model gives rise to expected effects on correlation times, $1/f$ spectra, and phase-space behavior.

While the model is not constructed to emulate sweeping time decorrelation, it is evident that introducing wave activity has the expected effect on the time decorrelations in the computed solutions, in absence of sweeping (see Fig. 10), although the energy spectra maintain Kolmogorov scaling in the inertial range even after introducing the wave term (see Fig. 8).

We remark that this kind of approach is not entirely new in plasma physics and our scheme is similar to that described in TenBarge *et al.* [4]. Our model validates and generalizes the scheme even further. Plasma systems with system sizes much larger than kinetic scales show MHD-like behavior at large scales but small-scale properties like dissipation are described by kinetic physics. Even with state of the art computational resources, Particle In Cell (PIC) kinetic simulations with some of the largest system sizes only begin to probe near the edge of inertial range. The study presented in this paper may be useful to couple kinetic simulations to large-scale fluid driving.

The arguments presented here do not capture the sweeping effects properly. The smaller eddies in a turbulent system are swept away by the larger eddies before any significant deformation takes place. As a consequence, a sweeping or advection timescale ($\tau_s \sim k^{-1}$) comes into play apart from the local nonlinear time [57] (viscous dissipation timescale becomes important only in dissipation range). This effect induces a profound difference in the Eulerian statistics and the Lagrangian statistics (following fluid elements). Of course the present model, having only a single independent complex degree of freedom at each scale, is too simple to distinguish such Lagrangian effects [58]. A more complete model would be required to incorporate this level of realism. Whether this can be done with a relatively simple model remains to be established. Further, the arguments presented here do not produce the intermittency effects as observed in MHD. We are in the process of including such effects into a more advanced model like [2].

Here we concentrate mostly on turbulent plasma systems. The ideas presented here may be extended to other turbulent systems such as convective turbulence, stably stratified flows, rotating turbulence, etc. Our approach may be useful to model other chaotic phenomena such as stock market exchange, earthquake intensities, prices of commodities, etc.

ACKNOWLEDGMENTS

The authors thank Debanjan Sengupta and Sergio Servidio for fruitful discussions during the initial stage of the project, and Aadya Parashar for assistance with the manuscript. The authors are grateful to the two anonymous referees whose input helped to substantially improve the quality of the manuscript. This research is supported in part by NSF AGS-1063439 and AGS-1156094 (SHINE) and by NASA Grants No. NNX15AB88G (L.W.S.), No. NNX14AI63G (Heliophysics Grand Challenges), and No. NNX17AB79G (Heliophysics GI Program), and the Solar Probe Plus project under Subcontract No. SUB0000165 from the Princeton University ISOIS project.

[1] G. Uhlenbeck and L. Ornstein, Phys. Rev. **36**, 823 (1930).
[2] C. Beck, Phys. Rev. E **49**, 3641 (1994).
[3] R. Balescu, H. Wang, and J. H. Misguich, Phys. Plasmas **1**, 3826 (1994).
[4] J. TenBarge, G. Howes, W. Dorland, and G. Hammett, Comput. Phys. Commun. **185**, 578 (2014).
[5] T. Lee, Q. Appl. Math. **10**, 69 (1952).
[6] R. H. Kraichnan, J. Fluid Mech. **59**, 745 (1973).
[7] U. Frisch, A. Pouquet, J. Leorat, and A. Mazure, J. Fluid Mech. **68**, 769 (1975).
[8] R. H. Kraichnan and D. Montgomery, Rep. Prog. Phys. **43**, 547 (1980).
[9] J. V. Shebalin, Physica D **37**, 173 (1989).
[10] J. V. Shebalin, Geophys. Astrophys. Fluid Dyn. **107**, 411 (2013).
[11] S. Servidio, W. H. Matthaeus, and V. Carbone, Phys. Rev. E **78**, 046302 (2008).
[12] P. Dmitruk and W. H. Matthaeus, Phys. Plasmas **16**, 062304 (2009).
[13] S. R. Cranmer and A. A. van Ballegooijen, Astrophys. J. **594**, 573 (2003).
[14] B. D. G. Chandran, Phys. Rev. Lett. **95**, 265004 (2005).
[15] B. D. G. Chandran, Phys. Rev. Lett. **101**, 235004 (2008).
[16] G. G. Howes, K. G. Klein, and J. M. TenBarge, arXiv:1404.2913.
[17] K. G. Klein, G. G. Howes, J. M. TenBarge, S. D. Bale, C. H. K. Chen, and C. S. Salem, Astrophys. J. **755**, 159 (2012).
[18] W. H. Matthaeus, S. Oughton, K. T. Osman, S. Servidio, M. Wan, S. P. Gary, M. A. Shay, F. Valentini, V. Roytershteyn, H. Karimabadi, and S. C. Chapman, Astrophys. J. **790**, 155 (2014).
[19] P. Dmitruk, L. J. Milano, and W. H. Matthaeus, Astrophys. J. **548**, 482 (2001).
[20] S. Chandrasekhar, Rev. Mod. Phys. **15**, 1 (1943).
[21] M. von Smoluchowski, Phys. Z. **17**, 585 (1916).
[22] A. Einstein, Ann. Phys. (NY) **322**, 549 (1905).
[23] P. Dmitruk, W. H. Matthaeus, L. J. Milano, S. Oughton, G. P. Zank, and D. J. Mullan, Astrophys. J. **575**, 571 (2002).
[24] M. Hossain, P. C. Gray, D. H. Pontius, W. H. Matthaeus, and S. Oughton, Phys. Fluids **7**, 2886 (1995).
[25] T. de Kármán and L. Howarth, Proc. R. Soc. London, Ser. A **164**, 192 (1938).
[26] M. Wan, S. Oughton, S. Servidio, and W. H. Matthaeus, J. Fluid Mech. **697**, 296 (2012).
[27] B. R. Pearson, P.-A. Krogstad, and W. van de Water, Phys. Fluids **14**, 1288 (2002).
[28] P. Wu, M. Wan, W. H. Matthaeus, M. A. Shay, and M. Swisdak, Phys. Rev. Lett. **111**, 121105 (2013).
[29] T. N. Parashar, W. H. Matthaeus, M. A. Shay, and M. Wan, Astrophys. J. **811**, 112 (2015).
[30] A. N. Kolmogorov, Dokl. Akad. Nauk SSSR **30**, 301 (1941) [reprinted in Proc. R. Soc. London, Ser. A **434**, 9 (1991)].
[31] P. Dmitruk and W. H. Matthaeus, Astrophys. J. **597**, 1097 (2003).
[32] T. N. Parashar, S. Servidio, M. A. Shay, B. Breech, and W. H. Matthaeus, Phys. Plasmas **18**, 092302 (2011).
[33] P. Dmitruk and W. H. Matthaeus, Phys. Rev. E **76**, 036305 (2007).
[34] P. Dmitruk, P. D. Mininni, A. Pouquet, S. Servidio, and W. H. Matthaeus, Phys. Rev. E **83**, 066318 (2011).
[35] W. H. Matthaeus and M. L. Goldstein, Phys. Rev. Lett. **57**, 495 (1986).
[36] A. Bemporad, W. H. Matthaeus, and G. Poletto, Astrophys. J. **677**, L137 (2008).
[37] W. H. Matthaeus, B. Breech, P. Dmitruk, A. Bemporad, G. Poletto, M. Velli, and M. Romoli, Astrophys. J. Lett. **657**, L121 (2007).
[38] B. A. Breech, Topics in Solar Wind Turbulence, Ph.D. thesis, University of Delaware, 2008.
[39] M. K. Verma, Phys. Rep. **401**, 229 (2004).
[40] M. K. Verma, Phys. Plasmas **6**, 1455 (1999).
[41] S. A. Orszag and G. S. Patterson, Phys. Rev. Lett. **28**, 76 (1972).
[42] W. D. McComb, *The Physics of Fluid Turbulence* (Clarendon Press, Oxford, 1990).
[43] W. H. Matthaeus and M. L. Goldstein, J. Geophys. Res. **87**, 6011 (1982).
[44] S. Servidio, V. Carbone, P. Dmitruk, and W. H. Matthaeus, Europhys. Lett. **96**, 55003 (2011).
[45] R. Lugones, P. Dmitruk, P. D. Mininni, M. Wan, and W. H. Matthaeus, Phys. Plasmas **23**, 112304 (2016).
[46] J. V. Shebalin, W. H. Matthaeus, and D. Montgomery, J. Plasma Phys. **29**, 525 (1983).
[47] S. Oughton, E. R. Priest, and W. H. Matthaeus, J. Fluid Mech. **280**, 95 (1994).
[48] G. G. Howes and K. D. Nielson, Phys. Plasmas **20**, 072302 (2013).
[49] A. R. Bulsara and L. Gammaitoni, Phys. Today **49** (3), 39 (1996).
[50] P. Bak, C. Tang, and K. Wiesenfeld, Phys. Rev. A **38**, 364 (1988).
[51] C. Beck, Physica A **233**, 419 (1996).
[52] C. Beck, Physica D **103**, 528 (1997).
[53] C. Beck, Physica A **295**, 195 (2001).
[54] A. Hilgers and C. Beck, Europhys. Lett. **45**, 552 (1999).
[55] C. Beck and S. Miah, Phys. Rev. E **87**, 031002 (2013).
[56] S. Miah and C. Beck, Europhys. Lett. **108**, 40004 (2014).
[57] S. Chen and R. H. Kraichnan, Phys. Fluids A **1**, 2019 (1989).
[58] H. Tennekes, J. Fluid Mech. **67**, 561 (1975).